7-1994

Convection in Chemical Waves

D. A. Vasquez

J. M. Littley

J. W. Wilder

Boyd F. Edwards
Utah State University

Convection in chemical waves

Desiderio A. Vasquez,[1] Joseph M. Littley,[2] Joseph W. Wilder,[3] and Boyd F. Edwards[2]
[1]*Department of Physics, Indiana University–Purdue University at Fort Wayne, Fort Wayne, Indiana 46805-1499*
[2]*Department of Physics, West Virginia University, P.O. Box 6315, Morgantown, West Virginia 26506-6315*
[3]*Department of Mathematics, West Virginia University, P.O. Box 6310, Morgantown, West Virginia 26506-6310*
(Received 29 September 1993)

We present a theory for the vertical propagation of chemical waves near the onset of convection. Fluid motion, coupled to a standard reaction-diffusion mechanism for chemical wave propagation, determines the speed and shape of the reaction front in a two-dimensional slab. Our model is compared with experiments in capillary tubes. For tilted and horizontal tubes, fluid motion is always present with a corresponding increase in front speed.

PACS number(s): 47.20.Bp, 47.70.Fw, 82.20.Mj

I. INTRODUCTION

Chemical wave propagation has been the subject of numerous studies during the last two decades. The bulk of the theoretical work has focused on reaction-diffusion mechanisms describing phenomena such as reaction fronts, target waves, and spirals [1]. Nevertheless, a series of experiments has shown that fluid motion must be taken into account to explain some of the observed behavior. Experiments by Micke, Muller, and Hess [2] have established that convective rolls are associated with the propagation of target patterns in the Belousov-Zabhotinsky reaction. For the iron (II)–nitric acid system, Pojman and Epstein [3] observed that the speed of the front is very sensitive to the width of the tube in which the reaction is performed, thus concluding that the front propagation involves convection. Nagypal, Bazsa, and Epstein [13] have shown that the front speed in the chlorite-thiosulfate reaction varies with the direction of propagation with respect to the gravitational field. In experiments [4] by McManus and co-workers for the iodate–arsenous acid system, the reaction is performed inside capillary tubes of different diameters. If the front propagates downward, the front is flat and moves with constant speed independent of the diameter. For upward propagation, the front is flat for a small diameter (0.94 mm) and is curved for larger diameters (≥ 1.8 mm). For flat fronts, the ascending speed is the same as the descending speed, indicating that there is no convection for flat fronts. The ascending curved fronts have a higher speed due to convection. These experimental results are shown in Fig. 1. The experiments suggest the existence of a critical diameter for the onset of convection. The front is unstable to convection because the lighter reacted fluid is placed below the heavier unreacted fluid. For diameters smaller than this critical diameter there will be no convection, while convection will be present for larger diameters. A previous linear stability analysis indeed yields this critical diameter for the onset of convection [5,6]. However, linear stability cannot predict the increase of speed for these systems. The goal of the present work is to obtain the increase of speed and the change in shape near the onset of convection. We also study the front propagation for tilted tubes, for which convection is always present due to a horizontal density gradient.

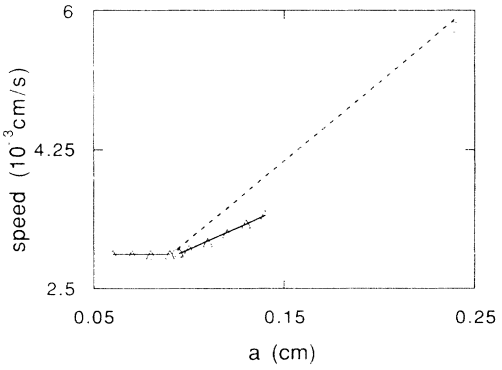

FIG. 1. Chemical wave velocity as a function of tube diameter or slab width. The circles represent the experimental data for cylinders and the triangles correspond to our numerical calculations for slabs. The horizontal axis a corresponds to the width of the slab and to the diameter of the cylinder, respectively. The broken line is a least squares fit to the experiments in cylinders and the solid line is a fit to the numerical results.

II. EQUATIONS OF MOTION

The equations that describe the time evolution of the system are the hydrodynamic equations of motion coupled to the one-variable reaction-diffusion equation [7] that governs the propagation of the front in the iodate–arsenous acid reaction with arsenous acid in stoichiometric excess [8]:

$$\frac{\partial \mathbf{V}}{\partial t}+(\mathbf{V}\cdot\nabla)\mathbf{V}=\frac{\rho-\rho_0}{\rho_0}\mathbf{g}-\frac{1}{\rho_0}\nabla P+\nu\nabla^2\mathbf{V}\ , \tag{1}$$

$$\nabla\cdot\mathbf{V}=0\ , \tag{2}$$

and

$$\frac{\partial c}{\partial t}+\mathbf{V}\cdot\nabla c=D\nabla^2 c-\alpha c(c-c_2)(c-c_3)\ . \tag{3}$$

Here, $\mathbf{V}$ is the fluid velocity, P is the reduced pressure and is related to the pressure by $P=p-p_0(g_x x+g_z z)$,

$\mathbf{g}=(g_x,g_z)$ is the acceleration of gravity ($g=980$ cm sec^{-2}), ν is the kinematic viscosity (9.2×10^{-3} cm^2 sec^{-1}), D is the molecular diffusivity (2.0×10^{-5} cm^2 sec^{-1}), c is the iodide concentration ($[I^-]$), c_2 is the initial concentration of iodate ($[IO_3^-]=5\times10^{-3}M$), c_3 is the ratio of two reaction rate constants $c_3=-k_a/k_b$, and $\alpha=k_b[H^+]^2([H^+]=10^{-2}M)$. The values of the reaction rate constants are [7,8] $k_a=4.50\times10^3M^{-3}\sec^{-1}$ and $k_b=3.45\times10^8M^{-4}\sec^{-1}$. The value of k_b ensures that the theoretical convectionless speed agrees with the observed speed. The density difference is included only where it modifies the large gravity term [9]. The heat equation is not included because the thermal front is thicker than the length scale for convection. This allows us to consider the temperature to be uniform and equal to the higher temperature of the reacted fluid. This assumption was verified explicitly for a linear stability analysis in which thermal effects were included [10]. The boundary conditions are no fluid velocity and no chemical flow at the vertical walls as well as no fluid velocity and fixed concentrations of iodide (zero for the unreacted fluid and c_2 for the reacted fluid) far away from the front. We allow a linear dependence of the density on the iodide concentration c:

$$\rho=\rho_0[1-\beta(c-c_2)] . \tag{4}$$

Here, ρ_0 is the density of the reacted fluid. The coefficient of linear expansion (β) is obtained from experimental measurements of the isothermal fraction density difference ($\delta=0.84\times10^{-4}$) between the unreacted and reacted fluids [9], $\beta=\delta/c_2$. Its value is given by $\beta=1.7\times10^{-2}$ g cm$^{-3}M^{-1}$. The small value of the fractional density difference justifies the use of the linear expansion Eq. (4).

A complete theoretical description of the experiments requires the use of a cylindrical geometry [6]. This problem is very complicated since it requires three components of the fluid velocity and a careful treatment of the singularity at the origin in cylindrical coordinates. Instead, we perform calculations on a two-dimensional slab. Using this geometry, we might expect to obtain semiquantitative results on the enhanced propagation speed above the onset of convection. This is much simpler since the velocity field can be replaced with a stream function in Cartesian coordinates. We can eliminate the reduced pressure and satisfy continuity identically by defining the stream function

$$V_x=\frac{\partial\psi}{\partial z} , \quad V_z=-\frac{\partial\psi}{\partial x} \tag{5}$$

and the vorticity

$$\omega=\nabla^2\psi . \tag{6}$$

This allows us to rewrite the equations as

$$\frac{\partial\omega}{\partial t}=\frac{\partial(\psi,\omega)}{\partial(x,z)}+\beta g_z\frac{\partial c}{\partial x}-\beta g_x\frac{\partial c}{\partial z}+\nu\nabla^2\omega , \tag{7}$$

$$\frac{\partial c}{\partial t}=\frac{\partial(\psi,c)}{\partial(x,z)}+D\nabla^2c-\alpha c(c-c_2)(c-c_3) , \tag{8}$$

where we have defined

$$\frac{\partial(f_1,f_2)}{\partial(x,z)}=\frac{\partial f_1}{\partial x}\frac{\partial f_2}{\partial z}-\frac{\partial f_2}{\partial x}\frac{\partial f_1}{\partial z} . \tag{9}$$

III. NUMERICAL METHOD

The set of equations defined by Eqs. (6), (7), and (8) was solved numerically. A fully explicit solution based on a finite difference scheme proved to be computationally intractable. Switching to an alternating direction implicit (ADI) scheme [12] did not result in a substantial improvement. Instead, simplification based on the results and methods employed on the linear stability analysis was used. In a linear stability theory of the transition to convection the chemical wave propagation was described in terms of the eikonal relation [5,6] involving the normal speed of the front (C), the flat front speed (C_0), and the front curvature ($\mathcal{K}$): $C=C_0+D\mathcal{K}$. This theory gave a very good approximation to the reaction-diffusion theory for the laterally unbounded problem. For the laterally bounded problem, namely the two-dimensional slab, the stream function was expanded in a complete set of orthonormal solutions [11] of

$$\frac{d^4}{dx^4}\mathcal{T}_m=\lambda_m^4\mathcal{T}_m \tag{10}$$

satisfying $\mathcal{T}_m=d\mathcal{T}_m/dx=0$ at $x=\pm\frac{1}{2}$. The eigenfunctions $\mathcal{T}_m$ are divided into two classes: C_m for even functions and S_m for odd functions. The functions and their eigenvalues λ_m are tabulated by Chandrasekar [11]. This expansion converges quite rapidly for the linear stability analysis [5]. The critical wall separation obtained for a one-term expansion was equal to 0.929 mm and for a three-term expansion the result was 0.928 mm. Based on this result we approximate the stream function by a truncated expansion:

$$\psi(x,z,t)=\sum_m A_m(z,t)\mathcal{T}_m(x/a) . \tag{11}$$

Here, a is the wall separation. Truncating the series provides a good approximation near the onset of convection, the regime of interest. Using this approximation and projecting onto $\mathcal{T}_n$, the two-dimensional Poisson equation [Eq. (6)] can be reduced to a set of coupled one-dimensional equations

$$(\omega|\mathcal{T}_n)=\frac{\partial^2}{\partial z^2}A_n(z,t)+\sum_m A_m(z,t)\left[\frac{d^2\mathcal{T}_m}{dx^2}\middle|\mathcal{T}_n\right] , \tag{12}$$

where

$$(f|\mathcal{T}_n)=\frac{1}{a}\int_{-a/2}^{a/2}f(x)\mathcal{T}_n(x/a)dx$$

for a given function $f(x)$. For an initial choice of iodide concentration, stream function, and vorticity, the time evolution equations [Eqs. (7) and (8)] provide the vorticity and the concentration after a small time step. This can be efficiently computed with an ADI method [12]. Once the vorticity is calculated, the stream function at the advanced time is obtained by first solving Eq. (12) for $A_n(z,t)$ and later using the expansion Eq. (11). For the

advanced time $t+\Delta t$, Eq. (12) determines a linear system of coupled ordinary differential equations in z, with matrix elements $(d^2\mathcal{T}_m/dx^2|\mathcal{T}_n)$ that are independent of z. The system can be easily decoupled by transforming onto a basis generated by the eigenvalues of this matrix. It is helpful to note that the matrix elements vanish if the eigenvalues $\mathcal{T}_n$ have opposite parity. Once the equations are decoupled, a mesh in the z direction is imposed and each equation is solved by inverting a banded matrix. The stream function is finally computed from the series Eq. (11). Since we are studying flow near the onset of convection we choose a four-term truncation of Eq. (11). It consists of the two even and the two odd functions with lowest eigenvalues λ_n. A one-term truncation also provided good results which will be discussed in the next section. The computations were performed on a 25×150 mesh which was 7.5 mm in length and up to 1.4 mm in width. The result did not change as the length was increased to 10 mm on a 25×200 mesh. The front was allowed to propagate a small distance and then the coordinate origin was shifted to center the front in the spatial domain, introducing "unreacted fluid" on top of the slab to cover for the shift. This procedure is justified as long as the top and bottom boundaries are away from the front.

IV. RESULTS

The initial conditions consist of no fluid flow anywhere. The initial iodide concentration profile was set to the convectionless reaction-diffusion front plus a small-amplitude random perturbation in the vicinity of the front. Simulations were then run for fronts propagating in slabs of different widths. For a width less or equal to 0.9 mm the perturbations die out, no fluid motion appears, and the chemical front becomes flat [Fig. 2(a)]. For widths greater or equal to 0.95 mm the perturbations grow in time, fluid motion appears, and the front changes its shape. After the decay of transients, the front shape, the fluid velocity, and the concentration gradients remain invariant in the comoving frame. The steady traveling wave solution for a particular value of the width a was used as the initial condition for the next higher value. The simulations for $a=1.3$ mm gave a convective front speed of 3.31×10^{-3} cm/s for the four-term truncation and 3.38×10^{-3} cm/s for the one-term truncation, illustrating the excellent convergence of successive truncations near the onset of convection. The steady convective chemical front is high on one side and low on the opposite side as shown in Fig. 2(b). From these simulations, we conclude that the predicted critical wall separation for the onset of convection is between 0.9 and 0.95 mm. This result is close to the linear stability analysis based on the eikonal relation which predicts a critical wall separation of 0.929 mm. This agreement helps to reaffirm the validity of the eikonal relation for bounded systems since no linear stability analysis has yet been performed using the reaction-diffusion equation on bounded systems. This also serves as a check of our numerical calculation. The curvature of the chemical front is due to a single convective roll that travels steadily with the front. The fluid rises on one side of the slab and falls on the other side as shown in Fig. 3.

The presence of a curved front with a single traveling convective roll separates this problem from the Rayleigh-Taylor problem. In that problem, two immiscible fluids are placed one on top of the other with surface tension providing the stabilizing mechanism. In our case, the reaction-diffusion mechanism changes one fluid into another yielding a front stable to small-wavelength, small-amplitude perturbations. This mechanism compensates for buoyancy and suppresses convection in very small tubes. In tubes of larger diameters, the interaction between the stabilizing (reaction-diffusion) and destabilizing (buoyancy) mechanisms leads to the traveling convective roll. This is not possible in the Rayleigh-Taylor problem because the two fluids are immiscible. This type of

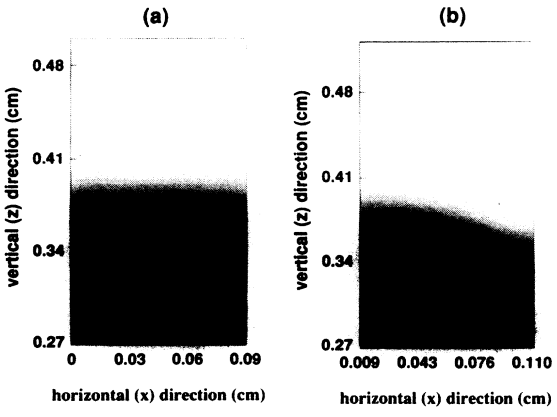

FIG. 2. The chemical front propagating upwards in a two-dimensional slab. The front is (a) flat for a slab width below 0.9 mm and it is (b) curved for larger widths. The change of curvature is due to the presence of convection. The lighter region represents zero iodate concentration (heavy unreacted fluid) and the dark region represents a concentration of $5\times10^{-3}M$ of iodate (lighter reacted fluid).

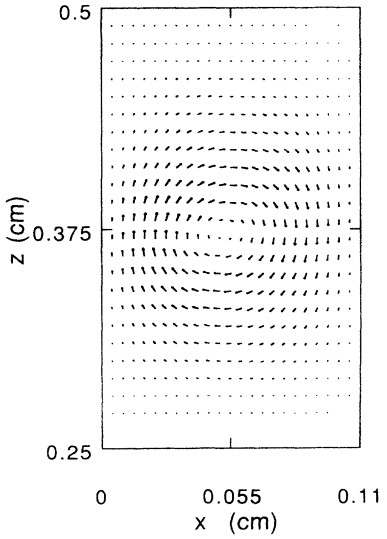

FIG. 3. Velocity field for a convective chemical wave. The convective roll travels upwards with the front and is steady in the comoving frame.

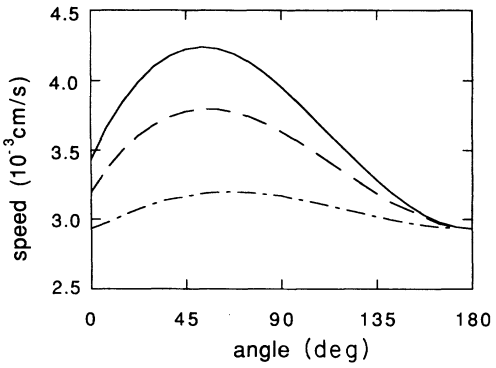

FIG. 4. Front speed as a function of the angle between the slab and the vertical direction. The solid line corresponds to a slab width of 0.14 mm, the broken line a slab width of 0.12 mm, and the broken-dotted line to a slab width of 0.085 mm.

convection is also different from Rayleigh-Bénard convection because the convective roll travels with constant speed and because the instability is driven by a nonlinear chemical composition profile and not by a linear temperature profile.

Our results for a two-dimensional slab are compared with experiments in cylinders in Fig. 1, which shows good semiquantitative agreement for the increase in speed due to convection. The experimental slope for the convective front speed as a function of diameter (Fig. 1) is approximately 1.98×10^{-2} sec^{-1} while the calculated slope is 1.07×10^{-2} sec^{-1}. While the shape of the front predicted by our model is different than the one observed previously in experiments [the model has the highest point lying near a wall as shown in Fig. 2(b)], recent work [14] which was performed to study the onset of convection has shown that near onset the front is nonaxisymmetric (as predicted by the model), with a transition to an axisymmetric front (the highest point of the chemical front in the middle of the tube) away from onset.

We also computed the speed of the front as the tube is tilted. In this case convection is always present since the tilted tube will impose a horizontal density gradient. Convection always enhances the speed of the chemical front. This is confirmed even for a slab width of 0.85 mm which is below the critical width for onset of convection in a vertical slab. In this case, the speed of the ascending front is the same as the speed of the descending front

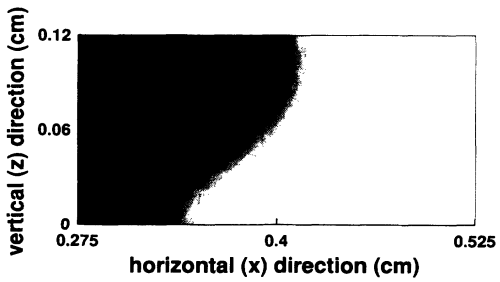

FIG. 5. The chemical front propagating to the right in a horizontal two-dimensional slab. The change of curvature is due to convection. The lighter region represents zero iodate concentration (heavy unreacted fluid) and the dark region represents a concentration of $5\times10^{-3}M$ of iodate (lighter reacted fluid).

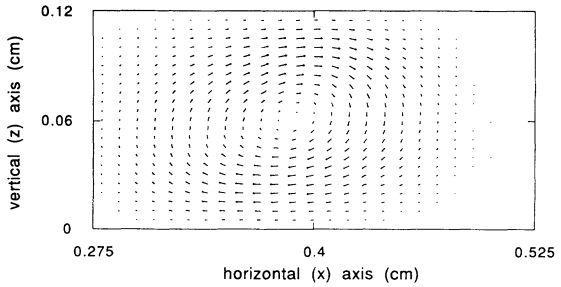

FIG. 6. Velocity field for a horizontal chemical wave. The convective roll travels to the right with the front and is steady in the comoving frame.

(Fig. 4) but is higher for any other direction. For slab widths of 0.12 and 0.14 mm, the velocity of ascending fronts is higher than descending fronts. The speed of the descending front is independent of the width because there is no convection. As the angle between the tube and the vertical direction is increased, the speed of the front increases as shown in Fig. 4. The speed reaches a maximum speed for an angle that depends on the width of the tube. For a slab of width 0.85 mm the angle is 65.8°, for a slab width of 1.2 mm the angle is 55.7°, and for a slab width of 0.14 mm the angle is 53.1°. This effect has been observed experimentally by Nagypal, Bazsa, and Epstein [13] for fronts in the chlorite-thiosulfate reaction. They proposed a qualitative explanation: since the tilted tube provides a wider cross section for a horizontal plane, consequently convection appears as it does in wider tubes. However, the tilted walls inhibit motion in the vertical direction, effectively slowing the front. The competition of both effects provides an angle for maximum speed away from both the vertical and horizontal directions. While the nature of the convection is different in the chlorite-thiosulfate reaction from that in the arsenous acid reaction (it is double-diffusive convection instead of simple convection), a similar qualitative explanation can be made for this system. Fronts in the horizontal direction have considerably enhanced speeds and enhanced curvature due to convection. We show the chemical front propagating in a horizontal slab in Fig. 5. The front is curved in a way similar to the vertical convective

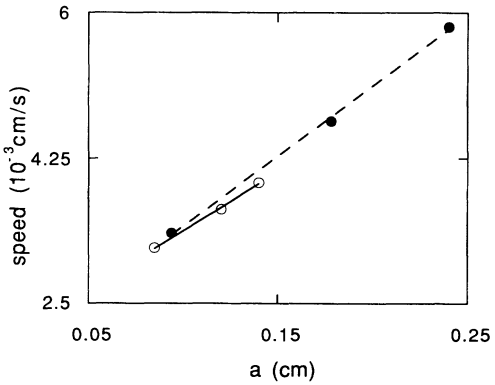

FIG. 7. Chemical wave velocity as a function of tube diameter or slab width for horizontal propagation. The open circles represent our numerical calculations and the closed circles are experimental results. The lines represent least squares fits to the data.

front. The curvature is explained by the associated convective roll (Fig. 6). We compare our results in the horizontal direction with experiments in horizontal cylinders [4] in Fig. 7. They show good semiquantitative agreement for the increase in speed due to convection. The experimental slope for the increase in convective front speed as a function of diameter (Fig. 7) is approximately 1.69×10^{-2} $\sec^{-1}$, while the calculated slope is $1.42\times10^{-2}\sec^{-1}$.

V. CONCLUSIONS

We have shown that the increase in speed observed in McManus's experiments can be explained by coupling hydrodynamics with the standard reaction-diffusion equations. The increase in speed is due to a steady convective roll that travels with the curved front. The shape of the front observed in these experiments is not the same as the one predicted by our model. This can be explained because linear stability analysis predicts a nonaxisymmetric state closer to the onset of convection than the regimes explored by McManus. Recent experiments, however, have shown that the front is nonaxisymmetric near onset, as predicted.

For horizontal fronts, our model compares well with experiments in horizontal cylinders providing a similar increase in front speed. The increase of speed is important since it nearly doubles the speed of the convectionless front in a cylinder of diameter equal to 2.4 mm. This shows that convective enhancements are important when comparing reaction-diffusion models with experiments. Our model also shows the existence of an angle for maximum front speed in tilted slabs. This could be studied experimentally by performing a series of experiments in which the front speed is measured as a function of the angle of inclination of sealed capillary tubes. Better agreement between the results presented here and such experiments might be achieved by carrying out the calculations in a cylindrical geometry. This problem requires treatment in three spatial dimensions which is considerably more difficult.

ACKNOWLEDGMENTS

Discussions with Kenneth Showalter are gratefully acknowledged. This work is supported in part by the National Science Foundation Grant No. RII-8922106 and the National Research Center for Coal and Energy.

[1] J. P. Keener and J. J. Tyson, Physica **32D**, 327 (1988); D. Barkley, M. Kness, and L. S. Tuckerman, Phys. Rev. A **42**, 2489 (1990).

[2] H. Micke, S. C. Muller, and B. Hess, Phys. Lett. A **141**, 25 (1989).

[3] J. A. Pojman and I. R. Epstein, J. Phys. Chem. **95**, 1306 (1991).

[4] T. McManus, Ph.D. thesis, West Virginia University, 1989); J. A. Pojman, I. R. Epstein, T. J. McManus, and K. Showalter, J. Phys. Chem. **95**, 1299 (1991).

[5] D. A. Vasquez, B. F. Edwards, and J. W. Wilder, Phys. Rev. A **43**, 6694 (1991).

[6] D. A. Vasquez, J. W. Wilder, and B. F. Edwards, Phys. Fluids A **4**, 2410 (1992).

[7] A. Saul and K. Showalter, in *Oscillations and Traveling Waves in Chemical Systems,* edited by R. J. Field and M. Burger (Wiley, New York, 1985), p. 419.

[8] D. A. Vasquez, J. W. Wilder, and B. F. Edwards, J. Chem. Phys. **98**, 2138 (1993).

[9] B. F. Edwards, J. W. Wilder, and K. Showalter, Phys. Rev. A **43**, 749 (1991).

[10] J. W. Wilder, B. F. Edwards, and D. A. Vasquez, Phys. Rev. A **45**, 2320 (1992); D. A. Vasquez, B. F. Edwards, and J. W. Wilder (unpublished).

[11] S. Chandrasekar, *Hydrodynamic and Hydromagnetic Stability* (Oxford University Press, London, 1961), Appendix V.

[12] W. Press, B. Flannery, S. Teukolsky, and W. Vetterling, *Numerical Recipes* (Cambridge University Press, Cambridge, 1986).

[13] I. Nagypal, G. Bazsa, and I. R. Epstein, J. Am. Chem. Soc. **108**, 3635 (1986).

[14] J. Masere, D. A. Vasquez, B. F. Edwards, J. W. Wilder, and K. Showalter , J. Phys. Chem. (to be published).

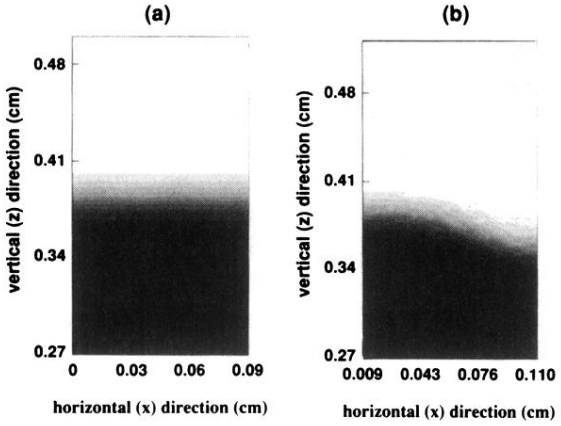

FIG. 2. The chemical front propagating upwards in a two-dimensional slab. The front is (a) flat for a slab width below 0.9 mm and it is (b) curved for larger widths. The change of curvature is due to the presence of convection. The lighter region represents zero iodate concentration (heavy unreacted fluid) and the dark region represents a concentration of $5\times10^{-3}M$ of iodate (lighter reacted fluid).

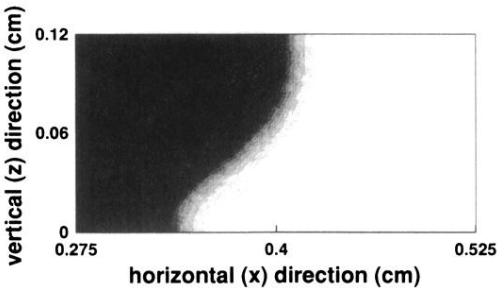

FIG. 5. The chemical front propagating to the right in a horizontal two-dimensional slab. The change of curvature is due to convection. The lighter region represents zero iodate concentration (heavy unreacted fluid) and the dark region represents a concentration of $5\times10^{-3}M$ of iodate (lighter reacted fluid).